Concept To Estimate Regional Inhalation Dose of Industrially Synthesized Nanoparticles

Antti J. Koivisto,[†,*] Mikko Aromaa,[‡] Jyrki M. Mäkelä,[‡] Pertti Pasanen,[§] Tareq Hussein,[⊥,∥] and Kaarle Hämeri[∥]

[†]Nanosafety Research Center, Finnish Institute of Occupational Health, Topeliuksenkatu 41 a A, FI-00250 Helsinki, Finland, [‡]Aerosol Physics Laboratory, Department of Physics, Tampere University of Technology, P.O. Box 692, 33101 Tampere, Finland, [§]Department of Environmental Science, University of Eastern Finland, P.O. Box 1627, 70211 Kuopio, Finland, [⊥]Department of Physics, Faculty of Science, University of Jordan, Amman, 11942 Jordan, and [∥]Department of Physics, University of Helsinki, P.O. Box 64, 00014 Helsinki, Finland

ABSTRACT The use of nanoparticles (NPs) in industry is increasing rapidly, but knowledge of the occupational health and safety aspects of NPs is still limited. This is because quantitative NP exposure levels are scarce, and the metrics to describe doses are unclear. This study presents one method for estimating workers' calculated regional inhalation dose of deposited particles from size-fractionated concentrations. It was applied to estimate workers' regional inhalation dose rates and doses separately for NPs and NPs with background particles during NP synthesis. Dose analysis was performed in units of particle number (particles and particles min^{-1}), active surface area (μm^2 and μm^2 min^{-1}), and mass (ng and ng min^{-1}) for three respiratory regions: head airways, tracheobronchial, and alveolar. It was found that in NP synthesis NPs were deposited mainly in the alveolar region in all units. However, when the dose of all particles was examined, it was found that dose and the main deposition region were mainly defined by the synthesized NPs for particle number, as active surface area was described by both NPs and background particles, and mass by background particles. This study provides fundamental data for NP inhalation exposure risk assessment, regulations, dose metrics for NP synthesis, and a basis for defining metrics of dose–biological response and helps us understand the magnitude of doses in NP synthesis. It also illustrates the necessity to obtain size-fractionated measurements of NP concentrations to support accurate dose estimation.

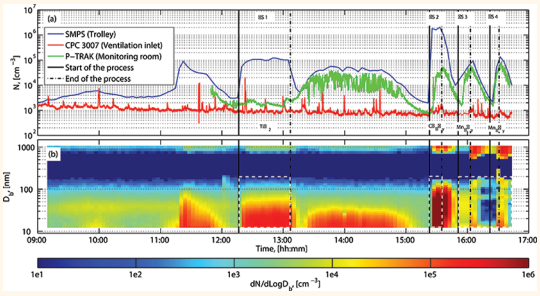

KEYWORDS: aerosol · inhalation exposure · dose estimate · nanoparticle · occupational hygiene

The rapidly increasing production and use of manufactured nano-objects (MNOs), such as nanoparticles, nanofibers, and nanoplates,[1] has created a demand to regulate the potential exposure of workers to MNOs.[2,3] Therefore, measurements at the workplace are needed for risk assessment in order to estimate the relevant exposure scenarios and exposure pathways of MNO uptake. Approximately 20 published studies currently exist on the concentration levels of MNOs in workplace air.[4] However, comparison of these studies is difficult because the quantitative exposure levels for MNOs and estimates for the deposited dose are lacking. The common issue in these studies is that the fraction of background particles associated with MNO concentration is not well-known.[4] Workplace air background particle concentrations originate from the outdoors *via* ventilation and indoor sources.[5] The process itself may also produce particles other than the MNOs. The discrimination of the background particles from MNOs is usually challenging to do and requires knowledge of size-fractionated concentrations and electron microscopy analysis of particles sampled during the process. In this study, we assess the quantitative exposure levels to synthesized nanoparticles (NPs) and estimate workers' regional inhalation dose of deposited particles.

We studied particle emissions from a liquid flame spray process (LFS) in which NPs were synthesized by atomizing a liquid precursor in a high-temperature flame. At high temperatures, the precursor droplet evaporates and subsequent reactions produce metal or metal oxide vapors which nucleate to the final particulate form. The LFS process is described in detail by Tikkanen *et al.*[6] and Mäkelä *et al.*[7] It is a widely used method for synthesizing NPs *in situ*, as it is stable, easy to control, and production yield can be extremely high. For example, Stark *et al.*[8] produced up to 200 g/h TiO_2 NPs with a single flame nozzle. A high temperature allows the use of a wide range of different precursors to produce NPs. These NPs can be modified in various ways. For example, Stark *et al.*[9] used a similar flame spray pyrolysis

* Address correspondence to joonas.koivisto@ttl.fi.

Received for review October 7, 2011 and accepted December 29, 2011.

Published online December 29, 2011
10.1021/nn203857p

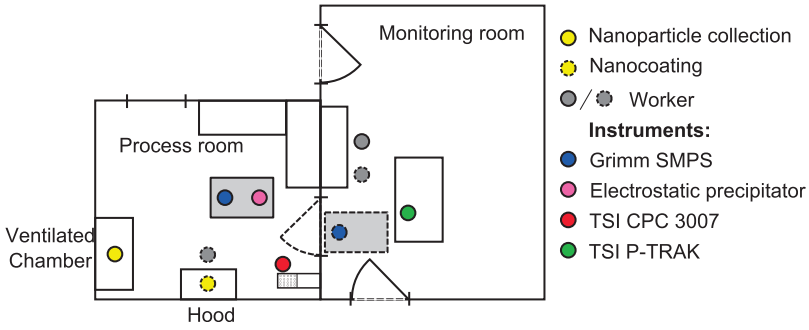

Figure 1. Process environment. Solid circle, door, and trolley lines refer to NP collection. Dashed lines refer to nanocoating.

technique to produce coated NPs by using mixed precursors, and Strobel *et al.*[10] produced aggregates with several types of NPs by using two or more flame nozzles. These advantages mean that the flame-based processes are very promising for synthesizing NPs in industry.

We took aerosol concentration measurements during the LSF process in two different applications: nanoparticle collection and nanocoating. The nanocoating was performed in an open space under a hood to create the worst case scenario of worker exposure. The synthesized NPs were discriminated from background particles by interpreting activity, time, and size-fractionated concentration profiles. Particle composition and morphology was defined from electron micrographs sampled from air during the processes. We studied inhalation exposure by quantifying regional inhalation dose rates in terms of particle number, active surface area, and mass concentration, where NPs and background particles were examined separately. These three metrics are considered necessary for NP risk assessment.[11] Active surface area and mass concentrations were defined from particle mobility size distributions by using existing conversion methods that appropriately account for factors such as particle shape and effective particle density.[12,13] During the past decade, a great deal of discussion has focused on the metrics that best describe exposure to NPs.[11,14,15] This study presents the contribution of NPs, and the contribution of background particles including NPs, to concentration and regional dose for these three metrics. The regional inhalation dose helps to estimate which physical quantity of synthesized NPs may be the biologically relevant attribute.[11,16,17] Furthermore, the results can be used for dose–risk characterization, as Ling *et al.*[18] did when estimating the doses received by workers in titanium dioxide[19] and carbon black[20] NP production plants.

Process Environment and Work Sessions. Figure 1 shows the process environment with information on the process layout, workers' positions during production, and the locations of instruments. The door between the process room and the monitoring room was closed during NP collection and open during nanocoating. The two doors between the monitoring room and the main building were open during NP collection and closed during nanocoating. The volume of the process room was 35.7 m^3, and the ventilation rate was 22 h^{-1}. The volume flow rate of supply air was 155 m^3 h^{-1}. The flow rate of exhaust air from the ventilated chamber and from the hood was 460 and 320 m^3 h^{-1}, respectively. We measured exhaust air flow rate when the process room and monitoring room doors were open, which resulted in maximum replacement air flow from the main building.

Measurements were taken over one working day between 9:30 and 17:00. Four work sessions (WS) were held during the working day:

WS 1: TiO_2 NP collection, 51 min.
WS 2: Cu_xO_y nanocoating 3 components, 4 min per component.
WS 3: Mn_xO_y nanocoating 3 components, 4 min per component.
WS 4: Mn_xO_y nanocoating 3 components, 3 min per component.

In the TiO_2 NP collection (WS 1), the flame nozzle was located in the 2.57 m^3 ventilated chamber, 1.0 m from the ceiling of the chamber, directly under the exhaust tube. During NP collection, a worker entered the process room five times. The worker wore a supplied-air facepiece respirator (Scott Proflow SC Automask Face Shield 063080 with Pro2000 CF32 A2B2E2K2-P3 R filter, CE certified to EN 12941:1998+A1:2003 class TH2A2B2E2K2P for which the nominal protection factor is 50), cotton clothing, regular shoes, and thermally insulated gloves. The average duration of one visit was 2 min.

During the nanocoating (WS 2, 3 and 4), one worker took a component from the monitoring room and went to the process room in which the coating was being performed. The flame was continuously on and was directed toward the component by a vertical steel cylinder. The hood was 1.0 m over the burner face, and the component to be coated was in the flame, 15 cm over the burner face. Another worker prepared components in the monitoring room. Both workers wore protective equipment as described above.

Workplace Air Particle Concentrations. Figure 2 shows (a) the particle concentration and (b) particle mobility size

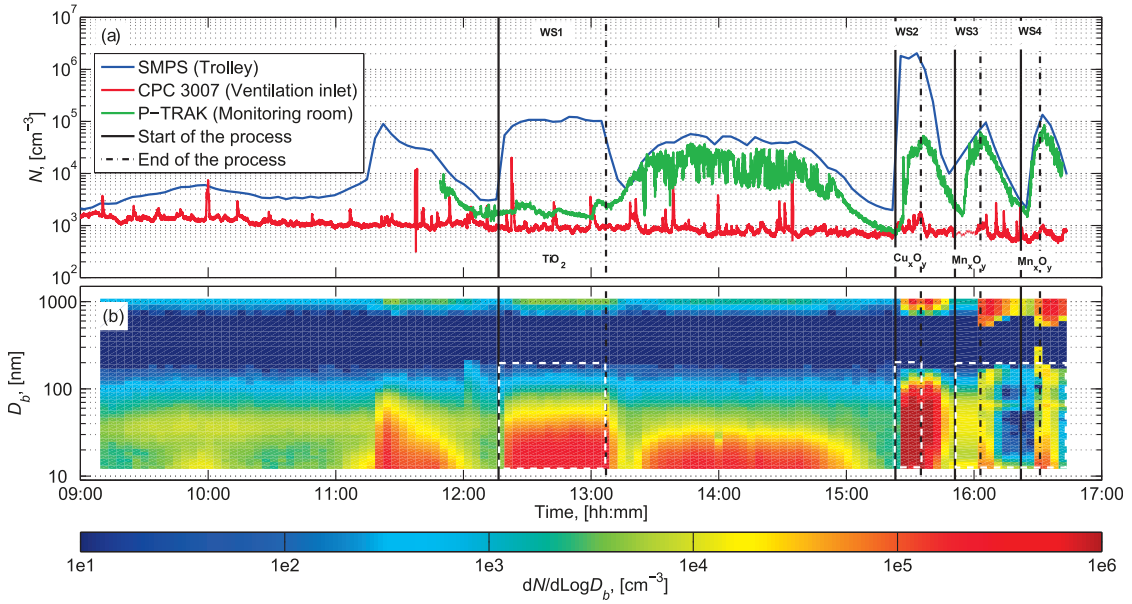

Figure 2. Time series of (a) particle concentrations and (b) particle mobility size distributions during the working day. White dashed rectangles in (b) delineate the concentrations of synthesized NPs to which the workers were exposed.

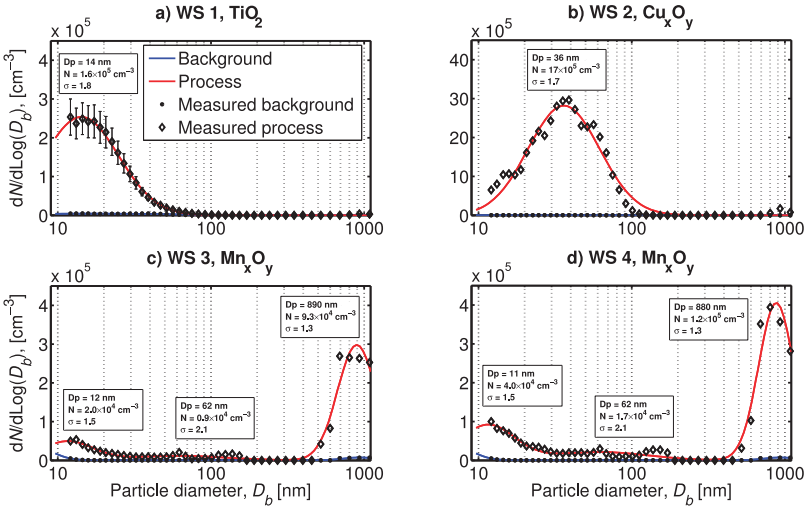

Figure 3. Particle mobility size distributions for each work session. In WS 1, mobility size distribution is an average (whiskers are one standard deviation), and in WS 2, 3, and 4, size distributions are taken from the peak concentration.

distribution time series measured during the working day. Average background particle concentration was defined from measurements before the NP collection at 12:15, and between WS 1 and 2 at 13:10 and 15:20. On average, it was 17 800(19 000) cm^{-3} in the process room, and 9100(8000) cm^{-3} in the monitoring room. The parentheses show one standard deviation of the concentration. Figure 2b shows that high variation in background particle concentration was mainly caused by concentration changes of particles smaller than 100 nm in diameter. These particles originated mainly from the main building because there was no activity in the working area, and the particle concentration of incoming ventilation air was 1100(600) cm^{-3}. Due to the high variation, the background particle concentration during the processes was defined from the concentration before the start and after the end of the work sessions. Subtraction was not performed because the background particle concentration was less than 3% of the process particle concentration (Figure 3).

Figure 3c,d shows that, during Mn_xO_y nanocoating, the particle size distribution was multimodal and dominated by fine particles (particle diameter 0.1 < D_p < 1 μm), with a particle size distribution mode of around 880 nm. Figure 2b shows that a similar fine particle mode was also present in Cu_xO_y nanocoating. We propose that these particles originated from the burning of impurities during the LFS process. The impurities may be located in the substrate,

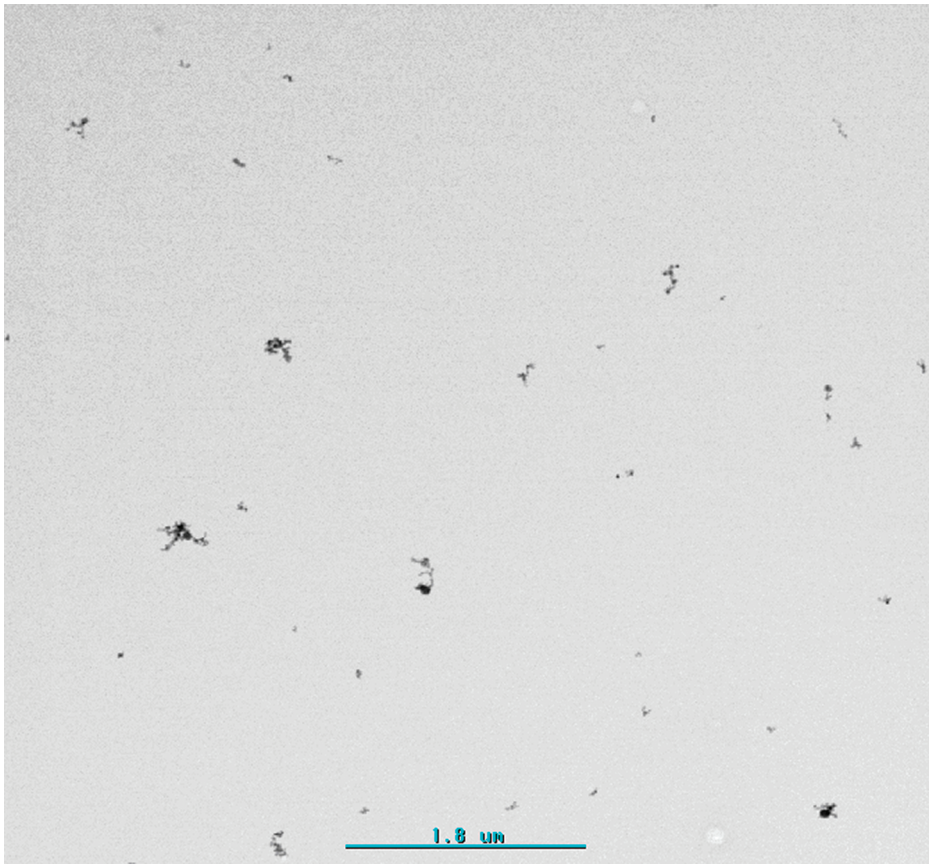

Figure 4. Micrograph of Cu_xO_y NPs sampled from the process room air.

substrate holder, or in components near the flame. These secondary combustion products were probably semivolatile particles which evaporated in an electron microscope vacuum chamber and were not detected in the electron micrograph (Figure 4). Figure 4 shows that nearly all Cu_xO_y NPs produced by the LFS process were less than 200 nm in diameter. The size of the TiO_2 NPs was similar (micrograph not shown). Thus we concluded that particles under 200 nm were NPs and that particles over 200 nm were background particles. Figure 3 supports this classification, when NP size distribution modes can be identified as being below 200 nm. The white dashed rectangles in Figure 2b delineate concentrations of the synthesized NPs to which the workers were exposed. The averages of these concentrations are listed in Table 1; they were used to calculate the workers' inhalation dose rates without taking the respirator protection into account. In Table 1, the monitoring room (MR) concentrations were averaged concentrations between the start of WS 3 and the end of measurements.

The log-normal particle size distributions in Figure 3 show that parts of the concentrations were not measured by the SMPS+C. This was most significant for WS 1, during which the SMPS+C particle concentration was underestimated by approximately 58%. MR concentrations measured by the SMPS+C apply only to the close vicinity of the measurement trolley (Figure 1). Figure 2a shows that the monitoring room particle concentrations measured by the P-Trak were lower than those measured by SMPS+C. This was due to the further location of the P-Trak from the process room than the SMPS+C, which results in higher dilution and increases loss of particles in number by deposition and coagulation. The difference was also due to the P-Trak 10 nm higher low particle detection limit.

The particle concentration during WS 1 was 101×10^3 cm^{-3}. This was similar to the concentration of 106×10^3 cm^{-3} measured by Demou *et al.*[21] in NP production with flame spray pyrolysis performed in a fume hood. Mäkelä *et al.*[22] also measured an increase of 10×10^3 cm^{-3} in particle concentration during TiO_2 NP synthesis in a similar environment. The difference in particle concentration may be explained by the NP collector located in the exhaust of the ventilated chamber. WS 2, performed under the hood, increased the average process room particle concentration to 1.83×10^6 cm^{-3} and active surface area to 13.6×10^3 μm^2 cm^{-3}. Mäkelä *et al.*[22] measured similar active surface area concentrations using a diffusion charger ranging from 1000 to 10×10^3 μm^2 cm^{-3} when, respectively, the flame nozzle was 40 and 80 cm below

TABLE 1. Room Concentrations in Particle Number, *N*, Active Surface Area, *S*, and Mass, *M*, and Estimated Regional Inhalation Dose Rates Not Taking Respirator Protection Factor into Account in Particle Number, $\dot{n}$, Active Surface Area, $\dot{s}$, and Mass, $\dot{m}$, Where Parentheses Show the Contribution of NPs[a]

unit/region	background	WS 1	WS 2	MR
N, $\times 10^3$ [cm^{-3}]	17.8 (99.0%)	101 (99.5%)	1830 (99.4%)	44.1 (25.0%)
$\dot{n}$, $\times 10^6$ [min^{-1}]	260 (99.0%)	1460 (99.5%)	20700 (99.2%)	530 (25.8%)
DF, [%]	58.8 (58.8)	57.5 (57.5)	42.6 (42.5)	48.1 (48.2)
head airways	11.8 (11.2)	11.2 (10.9)	10.5 (10.0)	53.9 (11.7)
tracheobronchial	19.7 (19.8)	19.4 (19.4)	17.5 (17.6)	9.8 (19.3)
alveolar	68.5 (69.0)	69.4 (69.7)	72.0 (72.4)	36.3 (69.0)
S, $\times 10^3$ [μm^2 cm^{-3}]	0.13 (23.0%)	0.46 (35.1%)	13.6 (51.6%)	16.2 (0.5%)
$\dot{s}$, $\times 10^9$ [μm^2 min^{-1}]	1.8 (18.2%)	6.2 (30.6%)	151.8 (39.7%)	204.4 (0.2%)
DF, [%]	52.4 (39.9)	51.6 (43.9)	42.1 (30.2)	50.1 (16.3)
head airways	60.0 (10.7)	52.4 (10.3)	47.8 (10.0)	68.6 (17.9)
tracheobronchial	8.9 (17.8)	10.2 (17.9)	10.2 (15.9)	6.7 (13.3)
alveolar	31.1 (71.5)	37.4 (71.8)	42.0 (74.1)	24.7 (68.8)
M, $\times 10^3$ [μg m^{-3}]	0.15 (0.3%)	0.44 (0.4%)	9.2 (1.2%)	19.6 (0.02%)
$\dot{m}$, [μg min^{-1}]	2.2 (0.15%)	6.3 (0.27%)	130 (0.65%)	263 (0.006%)
DF, [%]	57.1 (26.9)	56.7 (33.2)	55.2 (24.9)	53.2 (11.3)
head airways	70.7 (11.4)	70.5 (10.5)	69.9 (10.5)	69.6 (24.8)
tracheobronchial	7.0 (16.0)	7.0 (16.6)	7.0 (15.1)	6.9 (9.8)
alveolar	22.3 (72.6)	22.5 (72.9)	23.1 (74.4)	23.5 (65.4)

[a] Regional doses are expressed in percentages of the total dose fraction (DF) and are calculated for all particles and NPs (shown in parentheses). Monitoring room (MR) concentrations are averaged values between the start of WS 3 and the end of measurements.

the edge of the fume hood. This shows that high particle number and active surface area concentrations may occur in NP synthesis during the LFS process, and that the concentration depends on the position of the flame nozzle. Another example of high concentrations was measured by Heitbrink *et al.*[23] at an engine manufacturing plant. They measured peak particle concentrations of 8×10^6 and 2×10^6 cm^{-3} with respective active surface areas of 2000 and 1331 μm^2 cm^{-3} using a diffusion charger. However, the active surface area in MR was measured as 16.2×10^3 μm^2 cm^{-3}. This result is overestimated by high particle concentration at 880 nm, where the eq 1 conversion described below in the Methods section is not valid. The contribution of NPs to the active surface area was only 0.5%.

Table 1 shows that the average mass concentrations at WS 1 were 440 μg m^{-3}, at WS 2 9.2×10^3 μg m^{-3}, and in MR 16.2×10^3 μg m^{-3}. The mass originated mainly from fine particles over 700 nm in diameter. In WS 1 and 2, the mass from NPs was only 0.4 and 1.2%, respectively. Effective density usually decreases when mobility diameter is increased, which may affect the mass concentration defined from the SMPS+C measurements.[24] For example, if the effective density of the background particles was 0.4 g cm^{-3}, which corresponds to the effective density of diesel soot particles,[24] both the room mass concentration and mass inhalation dose rates in Table 1 would be 4.199(0.003) times lower. The contribution of particles with a diameter of less than 200 nm and with the same effective density of 1.7 g cm^{-3} would be 4.20(0.06) times higher. This would change the regional mass dose by a maximum of 4% in the alveolar region at WS 2 from 23.1 to 24%. This shows that even if the effective density of background particles was significantly lower, the contribution of NPs to room mass concentration would be very low, ranging from 5.0% at WS 2 to 0.09% in MR.

TABLE 2. Inhalation Dose Rates and Inhaled Dose of NPs When Workers' Use of Respiratory Protection with a Nominal Protection Factor of 50 Was Taken into Account

	background	WS 1	WS 2	MR
chemical composition		TiO_2	Cu_xO_y	Mn_xO_y
exposure time [min]	320	10	12	21
$\dot{n}$, $\times 10^6$ [min^{-1}]	260	29	410	2.8
n, $\times 10^6$	83800	292	4920	57.8
$\dot{s}$, $\times 10^3$ [μm^2 min^{-1}]	331	37.8	1200	9.1
s, $\times 10^3$ [μm^2]	106	0.38	14.5	0.19
$\dot{m}$, [ng min^{-1}]	3.44	0.34	16.9	0.32
m, [ng]	1100	3.4	203	6.7

Workers' Dose Estimate. Regional inhalation dose rates in Table 1 were calculated by multiplying the concentration by the particle deposition probability and the respiratory minute volume. The total dose fraction (DF) takes into account the fraction of particles deposited in the respiratory system during inspiration and expiration. For deposited particles, we calculated regional dose fractions. These values were calculated for all particles, including NPs and background particles, and for NPs.

Table 2 shows the workers' actual dose rates and inhaled dose of NPs that were calculated by multiplying Table 1 inhalation dose rates by the respirator protection factor. In this study, we used the respirator nominal protection factor (NPF, European standard: EN529, AIHA[25]), which is 50 for a TH2 class respirator.

This means that the maximum inward leakage of the respirator is 2%, and that this is assumed to be independent of particle size. This simplification defines that the regional dose and the DF were independent of the respirator. Thus, Table 1 regional dose fractions and the DF are the same for Table 2 respective inhalation dose rates. It must be noted that the real particle penetration is a strong function of particle size, where the maximum particle penetration is around 200 nm.[26] Thus, in order to obtain accurate dose estimation, the respirator workplace protection factor should be defined.[25]

The process room worker's estimated dose during 10 min of exposure at WS 1 was 292×10^6 TiO_2 particles, with an active surface of 380 μm^2 and a mass of 3.4 ng (Table 2). During 12 min of exposure at WS 2, the dose was 4.9×10^9 Cu_xO_y particles, with an active surface of 14.5×10^3 μm^2 and a mass of 203 ng (Table 2). In addition, the worker was exposed to Mn_xO_y NPs, which were measured only in the monitoring room. Depending on the WS and the unit to describe the dose, 69.7 to 74.4% of the deposited TiO_2 and Cu_xO_y NPs were deposited in the alveolar region (Table 1).

The monitoring room worker's estimated dose during 21 min of exposure was 57.8×10^6 Mn_xO_y particles, with an active surface of 190 μm^2 and a mass of 6.7 ng (Table 2). From the deposited Mn_xO_y, 65 to 69.0% of the NPs were deposited in the alveolar region (Table 1). However, in this, dose estimate was not included the NPs which were coagulated with the fine particle mode of around 880 nm (Figures 2b and 3c,d). According to the P-Trak, during WS 1, the monitoring room particle concentration did not increase, thus there was no significant exposure to TiO_2 NPs. However, P-Trak shows in Figure 2 that, during WS 2, the monitoring room particle concentration increased approximately as much as during WS 3 and 4. Thus the monitoring room worker was also exposed to Cu_xO_y NPs.

The results show that on average the dose in a work session ranged from 57.8×10^6 to 4.9×10^9 NPs, in spite of the fact that the duration of exposure was tens of minutes, and that the workers' protection was estimated by using the TH2 class respirator NPF (Table 2). However, during the working day, the workers' were exposed to background particles for 320 min without respirators. This exposure resulted clearly in the highest dose in all units. The process room worker's dose of background particles was 16, 7, and 5 times higher than the dose of TiO_2 and Cu_xO_y NPs in particle number, active surface area, and mass, respectively.

In the inhalation dose estimate, we assumed that the synthesized aerosol particles preserve their size in the lungs during inhalation. However, this might not be true especially if those particles accommodate water vapor under high relative humidity of 95.5% such as that in the human respiratory system. Therefore, the change in the particle size should be taken into account in accurate inhaled dose estimations. According to our knowledge, the hygroscopic growth of such synthesized aerosols is not well-known. If we consider extreme aerosols, such as those found in the urban atmosphere,[27−29] ultrafine particles between 10 and 100 nm in diameter have growth factor ranging between 1.25 and 2. We assume the NPs grow in a similar manner as urban aerosols. Recalling this, 15 nm TiO_2 particles in diameter would grow to around 20 nm where their DF would be reduced by 10%. Similarly, 35 nm Cu_xO_y NPs would have a growth factor around 1.5, at which their DF would be reduced by 22%. Thus, the exact growth factors of exposed metal oxides should be investigated to obtain the particle deposition accurately.

Metrics Describing NP Exposure. The metrics to describe the exposure to NPs should be sensitive to concentrations of NPs, and in addition, the influence of background particles on instrument detection should be small. When we examine the process room concentrations, Table 1 shows that the average contribution of NPs in concentrations of particle number was 99.5%, in active surface area 43.4%, and in mass 0.8%. Particle concentration was mainly defined by the concentration of NPs, and thus, it also defined the DF and the regional doses. For all particles, the average of all WSs' DF was 49% for particle number, 48% for active surface area, and 55% for mass, and for NPs, the average DF in respective units was 49.4, 30.1, and 23.1%. This shows that the DF of NPs with respect to the DF of all particles was nearly the same in particle number and decreased in active surface area by 21% and in mass by 48%. Thus, especially for active surface area and mass, the discrimination of NPs from background particles is necessary to avoid overestimation of the exposure. This may be difficult because 48% of the active surface area was defined by the background particles, as was over 98% of the mass. Table 1 shows that for NPs the main dose region for all units was in the alveolar region with an average dose fraction of 72.6%. The average of the main dose region for all particles was 70.7% for particle number in the alveolar region, 50.1 and 39.7% for active surface area in head airways and the alveolar region, respectively, and 70.2% for mass in head airways. This suggests that particle concentration best describes workers' NP dose in synthesis, and that when the particle moment of diameter is increased, the contribution of larger background particles to the metric is significantly increased. As a summary, regional dose analysis revealed that during the NP synthesis in the process room

- Particle concentration accurately described the dose of NPs: 99.5% of particles were NPs, and 70.7% of these were deposited in the alveolar region.
- The active surface area described the dose of NPs and background particles: 56.6% of the active surface area originated from background particles, and the main deposition regions were head

airways (50.1%) and the alveolar region (39.7%). With regard to NPs, 73.0% of the active surface area was deposited in the alveolar region.

- Mass concentration accurately described the dose of background particles: 99.2% of the mass originated from background particles, and 70.2% of the mass was deposited in the head airways. For NPs, 73.7% of the mass was deposited in the alveolar region.

This result is expected, but the magnitude for workplace aerosols has not been shown before. However, in the monitoring room, we can see that mainly the background particles originating from the process defined mainly the particle concentrations (Table 1). This shows that size-fractionated concentrations are required for discrimination of NP concentrations from the background particles. Only then may the exposure to NPs be defined accurately.

CONCLUSIONS

In summary, we have shown how regional inhalation dose of deposited NPs can be estimated in the presence of a background aerosol. The active surface area and mass concentrations were estimated from the size-fractionated particle concentrations by using the particle mobility diameter and effective density, respectively. We estimated workers' calculated regional inhalation doses of deposited NPs during NP synthesis. Results in this study enable evaluation of dose–effect relations to the exposed NPs when the toxicity of NPs is known. This information is needed to estimate risks related to the exposure in NP synthesis. We also found that the most informative metric to describe the dose of NPs in synthesis was particle concentration. However, that metric may not be useful quantity when exposure to larger MNOs is considered or post-processes of NPs where particles are highly agglomerated. This study shows the importance of measuring size-fractionated concentrations for dose estimation. It was required to discriminate NPs from background particles, to calculate size-fractionated active surface area and mass distributions, and to estimate regional dose of NPs.

METHODS

Nanoparticle Synthesis Using the LFS Process. Nanoparticle generator is described in more detailed by Mäkelä *et al.*[22] Three different types of NPs were synthesized from titaniumtetraisopropoxide diluted in isopropyl alcohol, copper nitrate diluted in water, and manganese sulfate diluted in water. A flame was used at a temperature of 2600 °C, with a hydrogen–oxygen (40:20 slpm) propellant. The overall reaction stoichiometries to produce TiO_2, Cu_xO_y, and Mn_xO_y NPs were

$$Ti(C_3H_7O)_4 \rightarrow TiO_2 + 4C_3H_6 + 2H_2O$$

$$Cu(NO_3)_2 \rightarrow Cu_xO_y + NO_2 + O_2$$

$$MnSO_4 \rightarrow Mn_xO_y + SO_2$$

The expected precursor feed rates were 23 mg min^{-1} for $Ti(C_3H_7O)_4$ and 4 mg min^{-1} for $Cu(NO_3)_2$ and $MnSO_4$. NP production rate was 40 mg min^{-1} in TiO_2 NP synthesis.[30] With regard to Cu_xO_y and Mn_xO_y, the NP production rate was the same order of magnitude. Depending on the process parameters, different oxides can be produced in the LFS synthesis. Copper and manganese oxide have several oxides that are producible through the LFS process. In this study, we measured a process that simulated a commercial coating, and therefore, the oxidation state is not relevant to measurements conducted for workplace safety.

Instrumentation. We measured the particle concentration of the incoming air using a TSI CPC 3007 condensation particle counter (TSI Incorporated, Shoreview, NM). The lower detection limit of the CPC 3007 was D_{50} = 10 nm, and sample flow rate was 0.7 L min^{-1}. The monitoring room particle concentration was measured using a TSI P-Trak condensation particle counter (TSI Incorporated, Shoreview, NM). The lower detection limit of the P-Trak was D_{50} = 20 nm, and sample flow rate was 0.7 L min^{-1}.

We used a sequential mobility particle size analyzer and counter (SMPS+C), Grimm Series 5.400 with a long differential mobility analyzer ("Vienna" Type U-DMA) to measure particle size distribution from 11.1 to 1082 nm (Grimm Aerosoltechnik, Dorfstrasse 9, 83404 Ainring, Germany). Large particles were removed by a preimpactor with a cut size of D_{50} = 1082 nm. The SMPS+C measurement time was set to 3 min with 28 s retrace intervals. The aerosol was neutralized by a ^{241}Am bipolar aerosol neutralizer. The aerosol sampling volume flow rate was 0.304 L min^{-1}.

A Grimm electrostatic precipitator (model #5.561) was used to sample aerosol particles in the size range of 1 nm to around 20 μm.[31] Sample volume flow was 0.46 L min^{-1}, and the voltage was 10 kV. TiO_2 and Cu_xO_y NPs were collected onto lacey carbon film-coated copper grids with 200 mesh (SPI West Chester, USA). The morphology and composition of the NPs were determined using a transmission electron microscope (TEM, JEOL model JEM 2010, Tokyo, Japan).

The SMPS+C and electrostatic precipitator were located on a measurement trolley that was in the process room during WS 1 and 2 and in the monitoring room during WS 3 and 4 (Figure 1). Instrument sampling inlets were positioned from 1.2 to 1.4 m above the floor level.

Unit Conversions from Mobility Diameter. Active[32] surface area, s, is defined as the surface of a particle that interacts with the surrounding gas molecules.[12,33] In theory, the measurement of active surface area measured using the diffusion charging method should be comparable with mobility analysis for particles between 20 and 180 nm.[12,33] Keller *et al.*[12] showed that, regardless of the shape of particles, the active surface area defined from mobility applies to particles up to 750 nm in diameter. The active surface area was calculated from the particle size distributions measured by the SMPS+C as described by Heitbrink *et al.*:[23]

$$s = \frac{3\pi\lambda D_b}{C_c(D_b)\delta} \quad (1)$$

where λ is the mean free path for air, 0.066 μm, and the scattering parameter δ for air is 0.905. The active surface area is proportional to particle diameter rather than to the square of the diameter.

Real mass m of the particle can be calculated from the effective density and mobility diameter of the particle:[13]

$$m = \rho_{eff}\frac{\pi}{6}D_b^3 \quad (2)$$

where ρ_{eff} is the effective density. The particle shape factor is implied in the effective density. The effective density was assumed to be 1.7 g cm^{-3} for both NPs and background particles.

This corresponds to an effective density of TiO_2 NPs synthesized with similar LFS process parameters.[34] Mean effective density of urban atmospheric aerosols are typically in the range of 1.5 to 2.2 g cm^{-3}.[35,36]

Inhalation Dose. This study considers the inhalation dose of deposited particles, surface area, and mass in the respiratory system during inspiration and expiration. Regional inhalation dose rate was defined by multiplying particle size concentrations measured by the SMPS+C by the ICRP human respiratory tract model deposition probability (International Commission on Radiological Protection, 1994), respiratory minute volume, and the exposure time. In this model, particles were assumed to preserve their size during inhalation. Respiratory minute volume was assumed to be 25 L min^{-1}, which corresponds to male respiration during light exercise. Regional dose was defined for head airways, the tracheobronchial region, and the alveolar region by using simplified deposition fraction equations for the ICRP model as described by Hinds.[37] These equations are expressed as a function of particle aerodynamic diameter D_a, which is related to mobility diameter D_b with a concept of effective density as[38]

$$D_a = D_b \sqrt{\frac{C_c(D_b)}{C_c(D_a)} \frac{\rho_{eff}}{\rho_0}} \quad (3)$$

where C_c is the slip correction factor for corresponding aerodynamic or mobility particle size[39] and ρ_0 is unit density (1 g cm^{-3}). The dose of active surface area and mass can be estimated by using the unit conversions from the mobility diameter.

Acknowledgment. The paper was supported by the Academy of Finland, FinNano-program, Engineered Nanoparticles: Synthesis, Characterization, Exposure and Health Hazards (NANOHEALTH)-project (project numbers 117 924 and 117 924).

REFERENCES AND NOTES

1. *Nanotechnologies - Terminology and Definitions for Nano-objects - Nanoparticle, Nanofibre and Nanoplate ISO TS 27687*; International Organization for Standardization, **2008**.
2. Brouwer, D.; Duuren-Stuurman, B.; Berges, M.; Jankowska, E.; Bard, D.; Mark, D. From Workplace Air Measurement Results toward Estimates of Exposure? Development of a Strategy To Assess Exposure to Manufactured Nano-Objects. *J. Nanopart. Res.* **2009**, *11*, 1867–1881.
3. Savolainen, K.; Pylkkänen, L.; Norppa, H.; Falck, G.; Lindberg, H.; Tuomi, T.; Vippola, M.; Alenius, H.; Hämeri, K.; Koivisto, J.; *et al.* Nanotechnologies, Engineered Nanomaterials and Occupational Health and Safety: A Review. *Saf. Sci.* **2010**, *48*, 957–963.
4. Brouwer, D. Exposure to Manufactured Nanoparticles in Different Workplaces. *Toxicology* **2010**, *269*, 120–127.
5. Hämeri, K.; Lähde, T.; Hussein, T.; Koivisto, J.; Savolainen, K. Facing the Key Workplace Challenge: Assessing and Preventing Exposure to Nanoparticles at Source. *Inhalation Toxicol.* **2009**, *21*, 17–24.
6. Tikkanen, J.; Gross, K. A.; Berndt, C. C.; Pitkänen, V.; Keskinen, J.; Raghu, S.; Rajala, M.; Karthikeyan, J. Characteristics of the Liquid Flame Spray Process. *Surf. Coat. Technol.* **1997**, *90*, 210–216.
7. Mäkelä, J. M.; Keskinen, H.; Forsblom, T.; Keskinen, J. Generation of Metal and Metal Oxide Nanoparticles by Liquid Flame Spray Process. *J. Mater. Sci.* **2004**, *39*, 2783–2788.
8. Stark, W. J.; Baiker, A.; Pratsinis, S. E. Nanoparticle Opportunities: Pilot-Scale Flame Synthesis of Vanadia/Titania Catalysts. *Part. Syst. Charact.* **2002**, *19*, 306–311.
9. Stark, W. J.; Wegner, K.; Pratsinis, S. E.; Baiker, A. Flame Aerosol Synthesis of Vanadia-Titania Nanoparticles: Structural and Catalytical Properties in SCR of NO by NH_3. *J. Catal.* **2001**, *197*, 182–191.
10. Strobel, R.; Baiker, A.; Pratsinis, S. E. Aerosol Flame Synthesis of Catalysts: A Review. *Adv. Powder Technol.* **2006**, *17*, 457–480.
11. Maynard, A. D.; Aitken, R. J. Assessing Exposure to Airborne Nanomaterials: Current Abilities and Future Requirements. *Nanotoxicology* **2007**, *1*, 26–41.
12. Keller, A.; Fierz, M.; Siegmann, K.; Siegmann, H. C.; Filippov, A. Surface Science with Nanosized Particles in a Carrier Gas. *J. Vac. Sci. Technol.* **2001**, *19*, 1–8.
13. Ristimäki, J.; Keskinen, J. Mass Measurement of Non-Spherical Particles: TDMA-ELPI Setup and Performance Tests. *Aerosol Sci. Technol.* **2006**, *40*, 997–1001.
14. Brouwer, D. H.; Gijsbers, J. H.; Lurvink, M. W. M. Personal Exposure to Ultrafine Particles in the Workplace: Exploring Sampling Techniques and Strategies. *Ann. Occup. Hyg.* **2004**, *48*, 439–453.
15. Maynard, A. D.; Kuempel, E. D. Airborne Nanostructured Particles and Occupational Health. *J. Nanopart. Res.* **2005**, *7*, 587–614.
16. Kreyling, W. G.; Semmler, M.; Möller, W. Dosimetry and Toxicology of Ultrafine Particles. *J. Aerosol Med.* **2004**, *17*, 140–152.
17. Oberdörster, G.; Oberdörster, E.; Oberdörster, J. Nanotoxicology: An Emerging Discipline Evolving from Studies of Ultrafine Particles. *Environ. Health Perspect.* **2005**, *113*, 823–839.
18. Ling, M.-P.; Chio, C.-P.; Chou, W.-C.; Chen, W.-Y.; Hsieh, N.-H.; Lin, Y.-J.; Liao, C.-M. Assessing the Potential Exposure Risk and Control for Airborne Titanium Dioxide and Carbon Black Nanoparticles in the Workplace. *Environ. Sci. Pollut. Res.* **2011**, *18*, 877–889.
19. Chen, C. C.; Bai, H. L.; Chein, H. M.; Chen, T. M. Continuous Generation of TiO_2 Nanoparticles by an Atmospheric Pressure Plasma-Enhanced Process. *Aerosol Sci. Technol.* **2007**, *41*, 1018–1028.
20. Kuhlbusch, T. A. J.; Neumann, S.; Fissan, H. Number Size Distribution, Mass Concentration, and Particle Composition of PM1, PM2.5, and PM10 in Bag Filling Areas of Carbon Black Production. *Occup. Environ. Hyg.* **2004**, *1*, 660–671.
21. Demou, E.; Stark, W. J.; Hellweg, S. Particle Emission and Exposure during Nanoparticle Synthesis in Research Laboratories. *Ann. Occup. Hyg.* **2009**, *58*, 829–838.
22. Mäkelä, J. M.; Aromaa, M.; Rostedt, A.; Krinke, T. J.; Janka, K.; Marjamäki, M.; Keskinen, J. Liquid Flame Spray for Generating Metal and Metal Oxide Nanoparticle Test Aerosol. *Hum. Exp. Toxicol.* **2009**, *28*, 421–431.
23. Heitbrink, W. A.; Evans, D. E.; Ku, B. K.; Maynard, A. D.; Slavin, T. J.; Peters, T. M. Relationships among Particle Number, Surface Area, and Respirable Mass Concentrations in Automotive Engine Manufacturing. *Occup. Environ. Hyg.* **2009**, *6*, 19–31.
24. Geller, M.; Biswas, S.; Sioutas, C. Particle Emission and Exposure during Nanoparticle Synthesis in Research Laboratories. *Aerosol Sci. Technol.* **2006**, *40*, 709–723.
25. AIHA, American Industrial Hygiene Association (AIHA), Respiratory Protection Committee: Respirator Performance Terminology [Letter to the Editor]. *Am. Ind. Hyg. Assoc. J.* **2002**, *63*, 132.
26. Shaffer, R. E.; Rengasamy, S. Respiratory Protection against Airborne Nanoparticles: A Review. *J. Nanopart. Res.* **2009**, *11*, 1661–1672.
27. Swietlicki, E.; Zhou, J.; Berg, O. H.; Martinsson, B. G.; Frank, G.; Cederfelt, S.-V.; Dusek, U.; Berner, A.; Birmili, W.; Wiedensohler, A.; *et al.* A Closure Study of Sub-Micrometer Aerosol Particle Hygroscopic Behaviour. *Atmos. Res.* **1999**, *50*, 205–240.
28. Väkevä, M.; Hämeri, K.; Aalto, P. P. Hygroscopic Properties of Nucleation Mode and Aitken Mode Particles during Nucleation Bursts and in Background Air on the West Coast of Ireland. *J. Geophys. Res. D* **2002**, *107*, 8104–8115.
29. Massling, A.; Stock, M.; Wiedensohler, A. Diurnal, Weekly, and Seasonal Variation of Hygroscopic Properties of Submicrometer Urban Aerosol Particles. *Atmos. Environ.* **2005**, *39*, 3911–3922.
30. Keskinen, H.; Mäkelä, J. M.; Aromaa, M.; Keskinen, J.; Areva, S.; Teixeira, C. V.; Rosenholm, J. B.; Pore, V.; Ritala, M.; Leskelä, M.; *et al.* Titania and Titania-Silver Nanoparticle

Deposits Made by Liquid Flame Spray and Their Functionality as Photocatalyst for Organicand Biofilm Removal. *Catal. Lett.* **2006**, *111*, 127–132.
31. Dixkens, J.; Fissan, H. Development of an Electrostatic Precipitator for Off-Line Particle Analysis. *Aerosol Sci. Technol.* **1999**, *30*, 438–453.
32. Fuchs, N. A. On the Stationary Charge Distribution on Aerosol Particles in a Bipolar Ionic Atmosphere. *Geofis. Pura E Appl.* **1963**, *56*, 185–193.
33. Ku, B. K.; Maynard, A. D. Comparing Aerosol Surface-Area Measurements of Monodisperse Ultrafine Silver Agglomerates by Mobility Analysis, Transmission Electron Microscopy and Diffusion Charging. *J. Aerosol Sci.* **2005**, *36*, 1108–1124.
34. Keskinen, H.; Mäkelä, J. M.; Aromaa, M.; Ristimäki, J.; Kanerva, T.; Levänen, E.; Mäntylä, T.; Keskinen, J. Effect of Silver Addition on the Formation and Deposition of Titania Nanoparticles Produced by Liquid Flame Spray. *J. Nanopart. Res.* **2007**, *9*, 569–588.
35. McMurry, P. H.; Xin, W.; Kihong, P.; Kensei, E. The Relationship between Mass and Mobility for Atmospheric Particles: A New Technique for Measuring Particle Density. *Aerosol Sci. Technol.* **2002**, *36*, 227–238.
36. Khlystov, A.; Stanier, C.; Pandis, S. N. An Algorithm for Combining Electrical Mobility and Aerodynamic Size Distributions Data When Measuring Ambient Aerosol. *Aerosol Sci. Technol.* **2004**, *38*, 229–238 (special issue of aerosol science and technology on findings from the fine particulate matter supersites program).
37. Hinds, W. C., Ed. *Aerosol Technology: Properties, Behavior, and Measurement of Airborne Particles*; Wiley: New York, 1999; pp 233−259.
38. Kelly, W. P.; McMurry, P. H. Measurement of Particle Density by Inertial Classification of Differential Mobility Analyzer-Generated Monodisperse Aerosol. *Aerosol Sci. Technol.* **1992**, *17*, 199–212.
39. Baron, P. A., Willeke, K., Eds. *Aerosol Measurements: Principles, Techniques and Applications*; Wiley-Interscience: New York, 2004; pp 705−749.